



Title	Design of chipless UWB RFID system using A CPW multi-resonator
Author(s)	Weng, Y; Cheung, SW; Yuk, TTI
Citation	IEEE Antennas and Propagation Magazine, 2013, v. 55 n. 1, p. 13-31
Issued Date	2013
URL	http://hdl.handle.net/10722/189078
Rights	IEEE Antennas and Propagation Magazine. Copyright © Institute of Electrical and Electronics Engineers.

Design of Chipless UWB RFID System Using A CPW Multi-Resonator

Y. F. Weng, S. W. Cheung, T. I. Yuk, and L. Liu

Department of Electrical and Electronic Engineering
The University of Hong Kong
Pokfulam Road, Hong Kong
Tel: +852 [28592711, 28592425, 28597098, 28592711]; Fax: +852 25598738
E-mail: [yfweng, swcheung, tiyuk, liuli]@eee.hku.hk

Abstract

In this paper, the design of a novel chipless ultra-wideband radio-frequency identification (UWB RFID) system is proposed. The system employs printable uniplanar chipless tags and a pair of high-gain reader antennas. The chipless tag is composed of two UWB monopole antennas, connected by a coplanar waveguide (CPW). The tag's ID is represented by a spectral signature in the UWB frequency range, and is created by a multi-resonator embedded on the coplanar waveguide. The detection of the tag's ID is based on using only the amplitude of the spectral signature, which significantly simplifies the complexity of detection. The reader employs two separate Vivaldi antennas – one for transmitting a vertically polarized signal, and the other for receiving a horizontally polarized signal – to reduce the mutual coupling between the uplink and downlink signals. Further reduction of mutual coupling is achieved by using a copper plate at the reader to separate the uplink and downlink signals. These two proposed methods together reduced the mutual coupling by 20 dB. The chipless RFID tag with eight coplanar waveguide resonators in a group and the reader antennas were designed using computer simulation, and fabricated on Rogers substrates for measurement. The results of studies in an anechoic chamber showed that the proposed UWB RFID system could achieve a reading range of larger than 30 cm, at least three times longer than the maximum distance of a similar system reported by others. This indicated that the proposed system has great potential for short-range item tracking at low cost.

Keywords: RFID; chipless RFID tag; chipless RFID systems; read range; uniplanar monopole antenna; ultra-wideband antenna; CPW resonator; vertical and horizontal polarization

1. Introduction

Because the automatic identification industry has been growing very fast in recent years, radio-frequency identification (RFID) technology has found more applications in various fields, including retail-chain management, asset identification, access control, movement tracking, and vehicle security [1, 2]. An RFID system mainly consists of three components: one or more identification tags (or transponders), a reader (transceiver) interface to communicate with the tags, and a data processing unit (host computer). The reader is usually fixed in position and connected to the host computer through wire lines (or via a wireless link), whereas the tags are the moving parts. The reader and the tags work as a wireless communication system. The tag is usually composed of an antenna and an application-specific integrated circuit (ASIC) for storing the tag's ID and data. For low-cost RFID systems, the tags are always passive,

and rely on the reader to provide energy in the form of EM signals for the ASIC to communicate with the reader. One of the main factors determining whether an RFID system should be deployed is the cost of the tags. Efforts have thus been put into research to develop chip-less RFID tags with no ASIC, in an attempt to lower the price of the entire RFID system [3-9].

In most existing RFID systems, such as those using low frequencies (from 100 kHz to 2 MHz), high frequencies (at 13.56 MHz), ultra-high frequencies (from 850 MHz to 950 MHz), and microwave frequencies (at 2.45 GHz and 5.8 GHz), the frequency bands used are quite narrow. Recently, increasing attention has been paid to applying ultra-wideband (UWB) technology to RFID applications [5-9], which could overcome some of the limitations of the current narrowband RFID technology. These limitations include small coverage area, insufficient ranging resolution for accurate localization,

sensitivity to interference, and scarce multiple-access capability [10, 11].

Currently, the only commercially available chipless RFID tags are based on surface-acoustic-wave (SAW) technology [4]. These tags are not fully printable or planar. Their piezoelectric nature and optical-lithography manufacturing process increase the cost. Recently, in [5-7], a fully printable chipless RFID tag was proposed for banknote applications. The size of the design was quite large. The detection of the tag's ID was based on both the amplitude and phase of the spectral signatures, which complicated the detection process. If only the amplitude of the spectral signature was used [5], the reading range was limited to only 10 cm.

In this paper, we present the design of a novel chipless UWB RFID system that employs fully printable, uniplanar, chipless tags. The chipless tag consists of two UWB monopole antennas, connected by a coplanar waveguide (CPW). A multi-resonator printed on the coplanar waveguide is used to represent the tag's ID in the form of a spectral signature across the UWB frequencies. The UWB monopole antenna studied in [12] and the multi-resonator studied in [13] were adopted in our design for the chipless tag. With the use of the UWB frequencies, many bits can be encoded into the spectral signatures for tag identification. However, in this study, just to prove our design concept, we used only eight resonators in the multi-resonator.

A Vivaldi antenna has the merits of high peak gain and theoretically unlimited instantaneous frequency bandwidth [14]. We thus used two Vivaldi antennas for transmitting and receiving signals in different polarizations, to reduce the mutual coupling between the uplink and downlink signals.

Both the chipless tag and the reader antennas were designed using the EM simulation tool CST *MWS*, and fabricated on Rogers substrate RO4350B for measurement. To further reduce mutual coupling between the uplink and downlink signals, we used a copper plate at the reader to separate the reader's transmitting and receiving antennas. As a result, we could use only the amplitude of the spectral signature for detection of the tag's ID. The use of amplitude for detection was not novel, and was already used in [5] and [6]. However, the novel idea proposed in this paper is a chipless UWB RFID system design, which uses only the amplitude (not the amplitude and phase together) of the spectral signature to simplify the detection complexity, yet achieving a reading range substantially larger than that reported before. Measurements of the chipless UWB RFID system were conducted inside an anechoic chamber using a programmable network analyzer (PNA), an Agilent E5071C, for signature detection. The results showed that the system could achieve a reading range of greater than 30 cm, at least three times longer than that reported in [5].

Several chipless RFID systems were proposed and studied by Preradovic, et al. in [5-7]. Although these systems employed concepts similar to ours, using chipless tags and resonators to create the spectral signatures to represent the tag's ID, there are major differences described as follows:

- A. The frequency band and detection method used: In our RFID system, we propose to use UWB frequencies, which are for unlicensed use with very low emission power. The chipless UWB RFID system is designed to operate in the frequency band from 3 GHz to 6 GHz. We propose to use only the amplitude of the spectral signature for detection of the tag's ID to simplify the detection process, yet achieving a much longer reading range than that reported in [5], which also used only amplitude for detection. Moreover, the authors in [5] designed a six-bit chipless tag to operate in the frequency band from 2 GHz to 2.5 GHz (which is not in the UWB frequency band). Although the authors mentioned that a 35-bit chipless tag was designed in the frequency band from 3 GHz to 7 GHz (in the UWB frequency band), they only presented the measured insertion loss of the tag, without giving any other results such as system measurement results. The studies in [6] were very similar to [5], and the only difference was the tags employed. In [7], the authors used amplitude and phase for detection, which was different from our proposed design. The results therefore could not be used for comparison, although the frequency band used in the design was in the UWB frequency band from 5 GHz to 10.7 GHz.
- B. Resonators: The resonators used in [5] and [6] were microstrip coupling spiral resonators, which required using both sides of the substrate. In our design, we propose to use a coplanar waveguide multi-resonator that needs to be etched only on one side of the substrate. This can lower the fabrication cost, which is one of the main factors determining whether an RFID system should be deployed. Although a coplanar waveguide structure was also used in [7], our design is quite different, and better. For example, our coplanar waveguide multi-resonator has an insertion loss of about 20 dB, much larger than the 8.5 dB for the design in [7].
- C. Programming the tag's ID: The authors in [5-7] used the idea of shorting a spiral turn of the tag's resonator to shift the resonant frequency to a higher value, which is also used in our design. However, they used spiral resonators, while we designed a new resonator that has much better performance in terms of frequency-shift range and insertion loss. Due to the limited frequency-shift range in [6], their resonator would have problems in using the whole UWB frequency band, as described later in Section 3. Our proposed resonator does not have such problems.

The paper is organized as follows. The basic concept of the proposed chipless UWB RFID system, the designs of the UWB monopole antennas used for the chipless tag, the coplanar waveguide multi-resonator, and the Vivaldi antennas used in the reader are all described in Section 2. The simulated and

measured results of the UWB antennas, the coplanar waveguide multi-resonators, and the Vivaldi antennas, together with the measured results of the whole chipless UWB RFID system in an anechoic chamber, are presented in Section 3. Section 4 concludes the studies.

2. Chipless UWB RFID System

2.1 Operating Principle of the Chipless UWB RFID System

The proposed chipless UWB RFID system used for this study is shown in Figure 1. It consisted of a chipless UWB RFID tag and a reader. The operating principle of the system was as follows. The reader transmitting antenna sent out a vertically polarized signal having a UWB spectrum in the downlink to the tag's receiving antenna. The signal received by the tag propagated along the coplanar waveguide to the other end, and was re-transmitted in horizontal polarization by the tag's transmitting antenna in the uplink to the reader's receiving antenna. As the signal traveled through the coplanar waveguide,

a spectral signature representing the unique ID for the tag was created by the coplanar waveguide multi-resonator. In our study, the multi-resonator, as shown in Figure 1, consisted of eight coplanar-waveguide resonators in a group, representing an eight-bit ID. At the reader, the received spectral signature was detected by a signal-processing unit, which was not part of our design. In our actual measurements on the prototype multi-resonator and the RFID system, a programmable network analyzer (Agilent E5071C) was used for extracting the spectral signature.

In the RFID system of Figure 1, the chipless tag used was passive, and relied on the power received from the reader in the downlink for re-transmission. The re-transmitted signal in the uplink received by the reader was quite weak. Since the tag had a small size, the reader's transmitting antenna had to be placed quite close to the reader's receiving antenna, and was transmitting a relatively stronger signal in the downlink. To reduce interference to the uplink signal due to mutual coupling, we used vertically and horizontally polarized signals in the downlink and uplink, respectively. To accomplish this, the reader consisted of a pair of planar Vivaldi antennas, placed perpendicularly to each other in such a way that the transmitting antenna transmitted a vertically polarized signal in the downlink, and the receiving antenna received a horizontally polarized signal in the uplink.

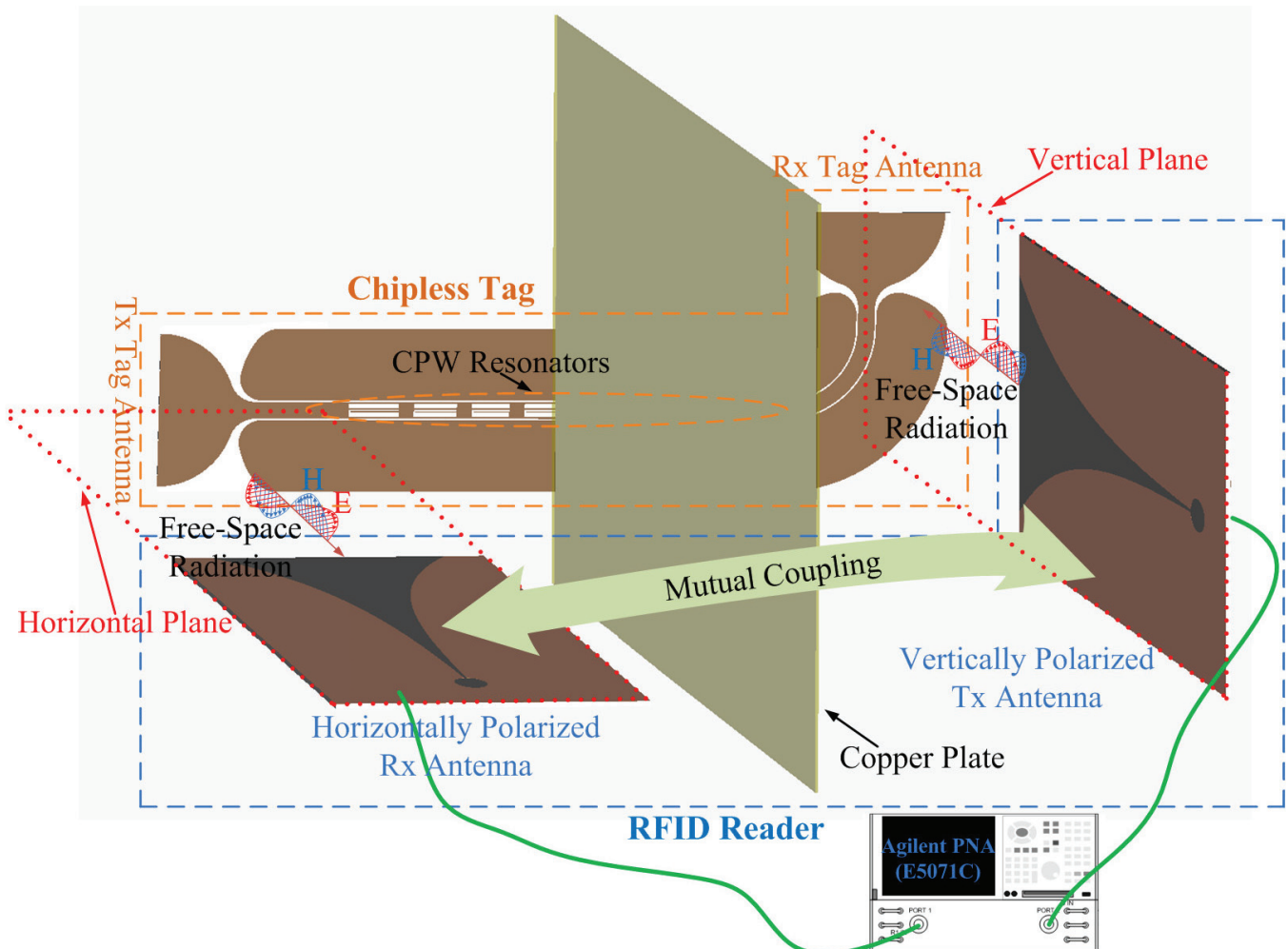


Figure 1. The operating principle of the chipless UWB RFID system.

As a result, the mutual coupling between the two antennas was significantly reduced. In Figure 1, the chipless tag had two UWB monopole antennas, one for receiving the vertically polarized signal and one for transmitting the horizontally polarized signal, connected together through a bent coplanar waveguide (CPW). To further reduce the mutual coupling, we placed a copper plate, with dimensions of 30 cm \times 40 cm, between the reader's transmitting and receiving antennas, as shown in Figure 1. The results in Section 3 showed that this combination could reduce the mutual coupling effect by about 20 dB.

2.2 Structure of Chipless Tag

The proposed chipless UWB RFID tag is shown in Figure 2. A printable uniplanar coplanar waveguide structure, with the merits of easy and low-cost fabrication [15], was employed. The antennas, the multi-resonator, and the coplanar waveguide were all etched on one side of the substrate. The two uniplanar UWB monopole antennas were connected together by a 50 Ω coplanar waveguide, embedded with eight coplanar waveguide resonators. The UWB antennas and multi-resonators were studied individually in [12] and [13], respectively. In the geometry of the tag shown in Figure 2b, the width, G , of the central conducting strip of the coplanar waveguide was 3.3 mm, and the gap, S , between the central conducting strip and the ground was 0.3 mm, resulting in a characteristic impedance of 50 Ω . The coplanar waveguide was bent 90° so that the tag could receive and transmit the corresponding polarized signals from and to the reader with low cross polarization. The ends of the coplanar waveguide had a half-elliptical shape, with a major radius of a and a minor radius of b , as shown in Figure 2a, to reduce the beam tilt of the antenna [16]. The small gaps between the central conducting strip and the ground of the coplanar waveguide near to the input of the radiator were very critical for impedance matching. They were therefore smoothed by using two arc shapes with radii of R_1 and R_2 [12].

Coplanar waveguide resonators in different structures have been studied before, e.g., the $\lambda/2$ open-ended coplanar waveguide resonators and $\lambda/4$ coplanar waveguide resonators used to design band-stop filters [17, 18]. However, those resonators were too large to be used in our design. Here, we propose a new and simple structure for the coplanar waveguide resonator, with a much smaller size, as shown in Figure 2c. Basically, the resonator was simply a rectangular slot with two open stubs from opposite sides. With this design, a group of eight resonators could be etched onto the coplanar waveguide of the tag. All these resonators had the same dimensions, except for the length, L_c^n , where $n = 1, \dots, 8$, was the index of the resonator, starting from the largest resonator to the smallest resonator. To reducing mutual coupling between resonators, the distance, L_a , separating adjacent resonators was set to 3 mm. The smallest dimension we could fabricate using the prototype machine in our laboratory was 0.1 mm. Therefore, for convenience in our design process and without compromising the fabrication

tolerance and compact size, we fixed the segment widths, w_2 and w_3 , to be 0.3 mm. Our results showed that the lengths, L_c and L_d , of the resonator could be used to set the resonant frequency. Moreover, shorting the two open stubs to the other sides by making $L_d = 0$ could shift the resonance to a much higher frequency, and, at the same time, substantially reduce the insertion loss (S_{21}). This property could be used to encode different bit patterns into the tags and, hence program the tags' IDs. One major advantage of this shorting property is that in the future, we may just use a fixed pattern of the multi-resonator having only strips (instead of open stubs) for printing the tags. We can then use a laser or other simple etching technique to create the gap of L_d , and hence to program different tags with different IDs.

The dimensions of the chipless UWB RFID tag are given in Table 1.

2.3 Structure of Reader Antenna

Using high-directivity and high-gain antennas in the reader can increase the reading range. The Vivaldi antenna, with a periodic and continuously scaled structure, theoretically has an unlimited instantaneous bandwidth, a significantly high peak gain, and linear polarization [19, 20], and so it was a perfect candidate for our reader antenna. Two identical Vivaldi antennas with a planar structure as shown in Figure 3 were designed for our reader. The directions of the E and H fields of the antenna as indicated in Figure 3a were same as those indicated in Figure 1. The antennas had a profile of an exponentially tapered slotline, ending with a circular-slotline cavity. The exponentially tapered profile was defined by the position of the origin, indicated as O in Figure 3a; the opening rate, r ; and the two coefficients, c_1 and c_2 [20]. These were related according to $y = c_1 e^{rx} + c_2$, where x was from 0 mm to 150 mm in our design. This profile served as the radiator of the antenna, and was etched onto one side of the substrate. For good impedance matching across the UWB frequency range, a linear-tapered stripline, etched on the other side of the substrate as shown in Figure 3b, was used for feeding the signal to the radiator. The stripline had a 90° bend, and was terminated with an arc-shaped stripline stub. All these dimensions were optimized for $S_{11} < -10$ dB across the UWB frequency range using computer simulation; they are listed in Table 2.

3. Results and Discussions

To validate our design concept, the UWB monopole antennas for the tag, the multi-resonator, and the reader antennas were individually fabricated on Rogers substrate RO4350B and measured. The complete RFID tag was also fabricated. The whole RFID system was studied in a 4 m \times 4 m \times 8 m anechoic chamber in our Radio Frequency Lab.

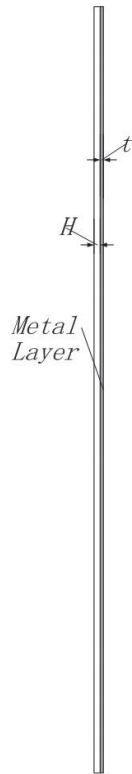


Figure 2a. A side view of the chipless UWB RFID tag.

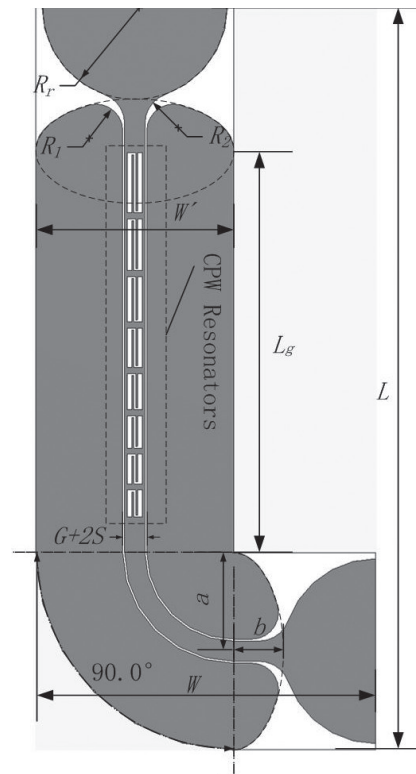


Figure 2b. A top view of the chipless UWB RFID tag.

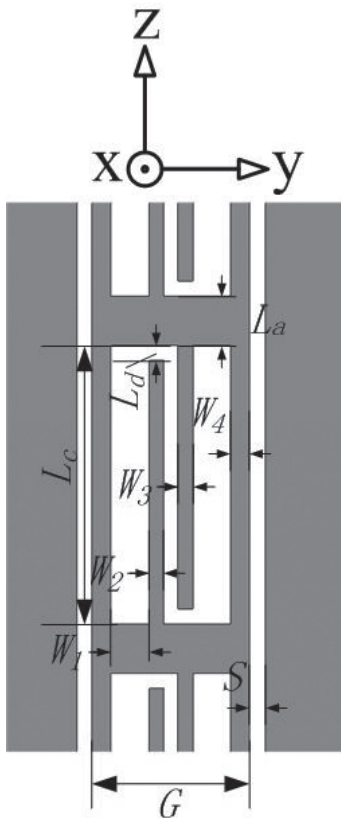


Figure 2c The coplanar waveguide resonator of the chipless UWB RFID tag.

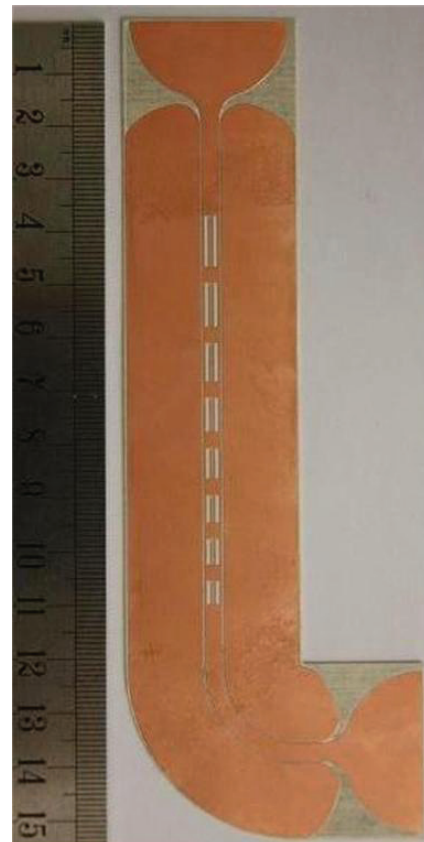


Figure 2d. The prototype of the chipless UWB RFID tag.

Table 1. The dimensions of the chipless UWB-RFID tag (mm).

L	154
W	55
W'	32
L_g	39.3
R_1	4.3
R_2	5
R_r	15
H	0.254
T	0.035
a	16
b	8
G	3.3
S	0.3
W_1	0.8
W_2	0.3
W_3	0.3
W_4	0.4
L_d	0.3
L_a	3
L_c^1	9.7
L_c^2	8.4
L_c^3	7.3
L_c^4	6.4
L_c^5	5.8
L_c^6	5.3
L_c^7	4.8
L_c^8	4.4

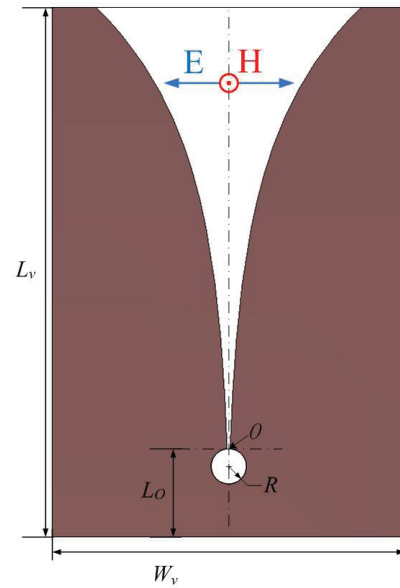


Figure 3a. A top view of the reader's antenna structure.

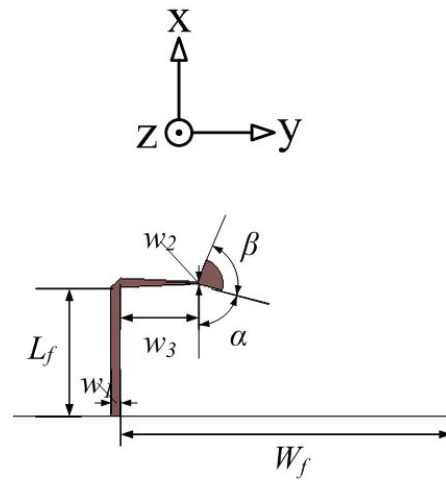


Figure 3b. A bottom view of the reader's antenna structure.



Figure 3c. The prototype of the reader's antenna.

Table 2. The dimensions of the reader's antenna (mm).

L_y	180
W_y	120
L_f	30
L_o	30
W_f	77.6
α	75°
β	85°
R	6
w_1	2.4
w_2	0.3
w_3	18
r	0.022
c_1	1.7
c_2	1.2

3.1 Tag Antennas

The UWB monopole antennas used in the RFID tag of Figure 2b were selected from our previous design [12, 13]. The prototyped antenna on a Rogers substrate is shown in Figure 4. The simulated and measured S_{11} of the antenna are shown in Figure 5. The antenna had an impedance bandwidth ($S_{11} \leq -10$ dB) from 3.06 GHz to over 10.82 GHz, fully satisfying the FCC UWB requirement. The small discrepancies between the simulated and measured results could be due to the tolerances in prototype fabrication and measurement, and also the SMA connector, which was not used in our simulation.

The simulated and measured radiation patterns of the antenna at the frequencies of 3 GHz, 5 GHz, and 11 GHz, in the xz and xy planes, are shown in Figure 6. It could be seen that the measured and simulated radiation patterns were in good agreement. In the xy plane, Figures 6a, 6c, and 6e showed that the radiation patterns were omnidirectional. In the xz plane, Figures 6b, 6d, and 6f showed that the radiation patterns had two nulls in the positive and negative z directions, typical for monopole antennas.

The radiation pattern of the antenna could be better seen using three-dimensional plots. The measured three-dimensional radiation patterns of the antenna at the frequencies of 3 GHz, 6 GHz, 8 GHz, and 11 GHz are shown in Figure 7. At the lower frequencies of 3 GHz and 6 GHz, Figures 7a and 7b showed that the antenna had approximately “apple-shaped” radiation patterns. At the higher frequencies of 8 GHz and 11 GHz, Figures 7c and 7d showed that the radiation patterns became slightly directional, with the main lobe pointing slightly upward. This was due to the planar structure of the monopole antenna, and the unbalance of the antenna’s radiator and ground plane [21]. All these radiation patterns showed two nulls in the z direction, as expected.

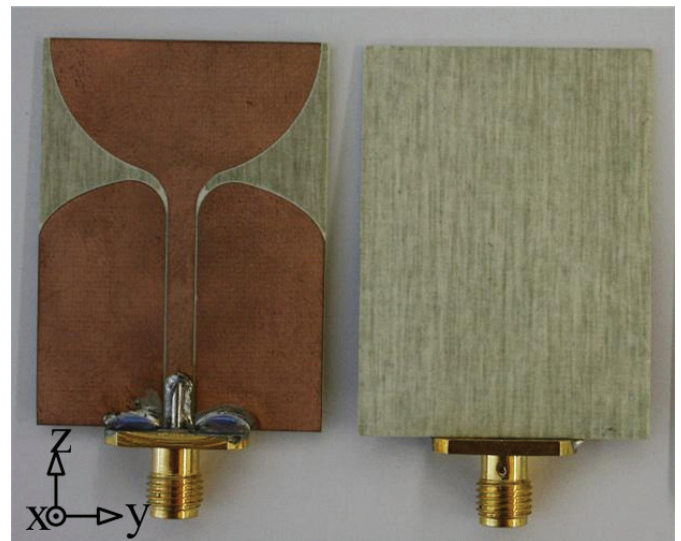


Figure 4. The prototype of the UWB monopole antenna.

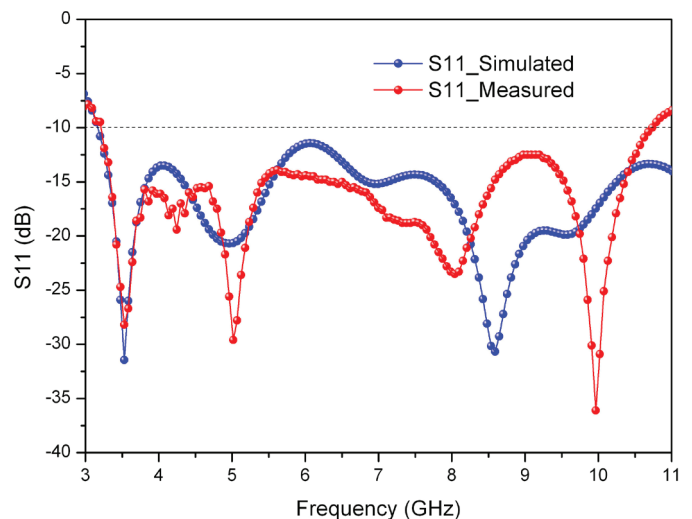


Figure 5. The measured and simulated S_{11} values for the UWB monopole antenna.

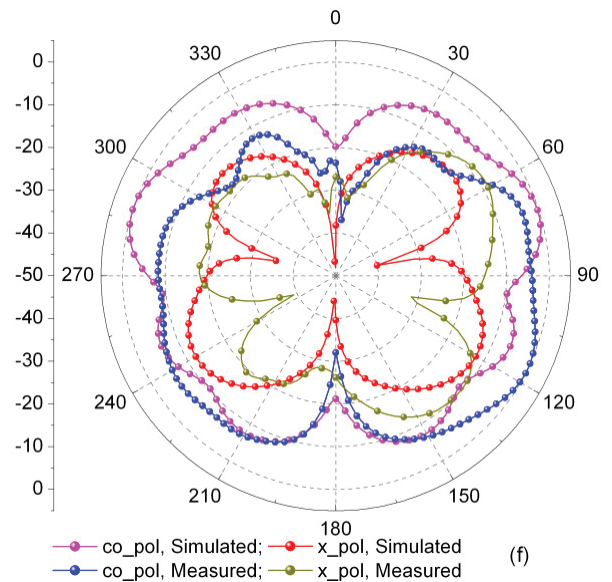
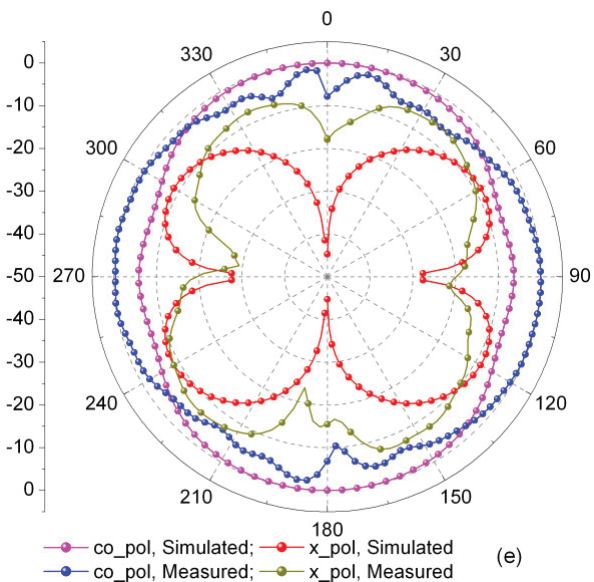
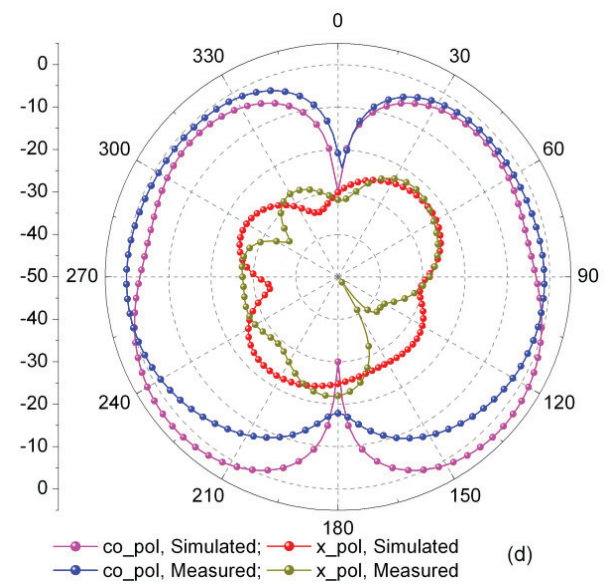
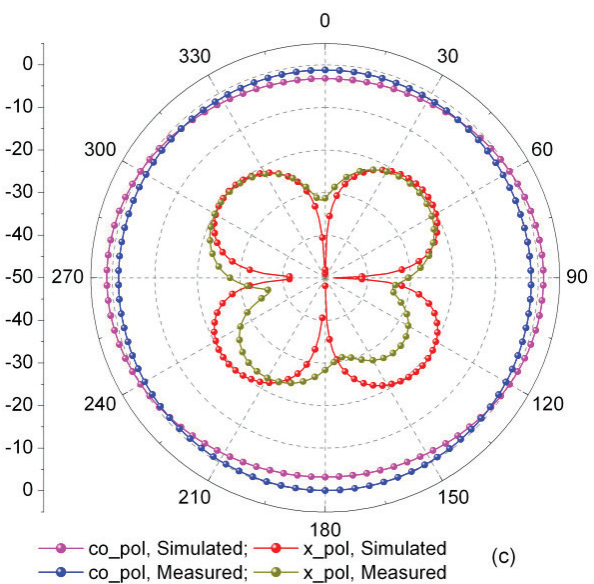
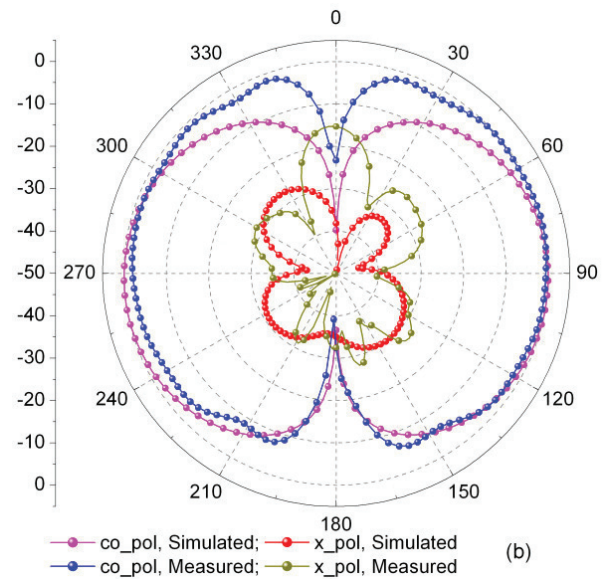
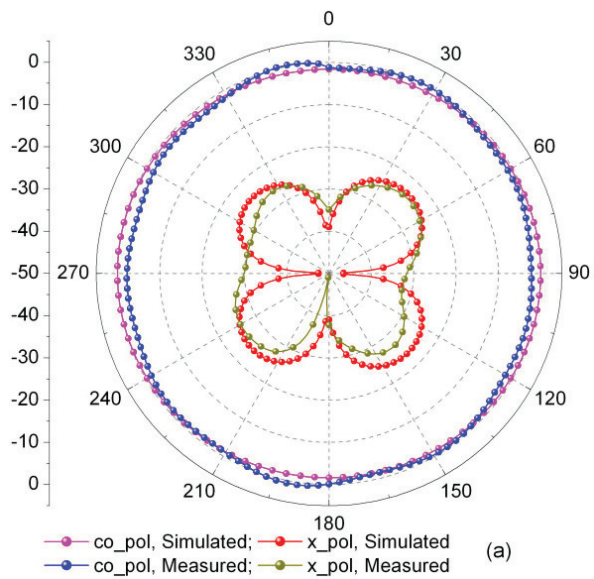
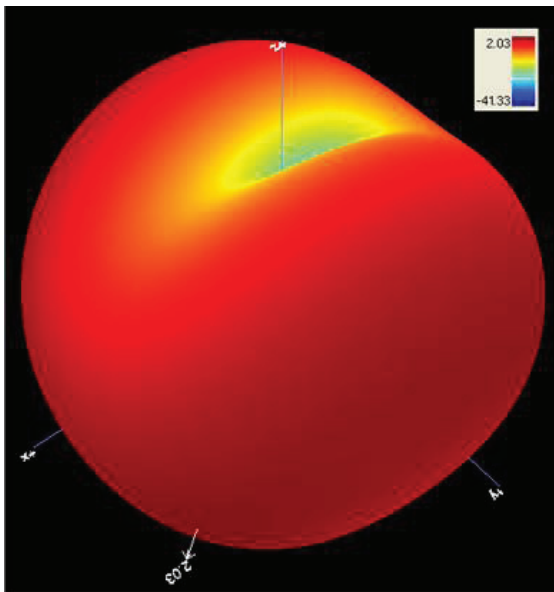
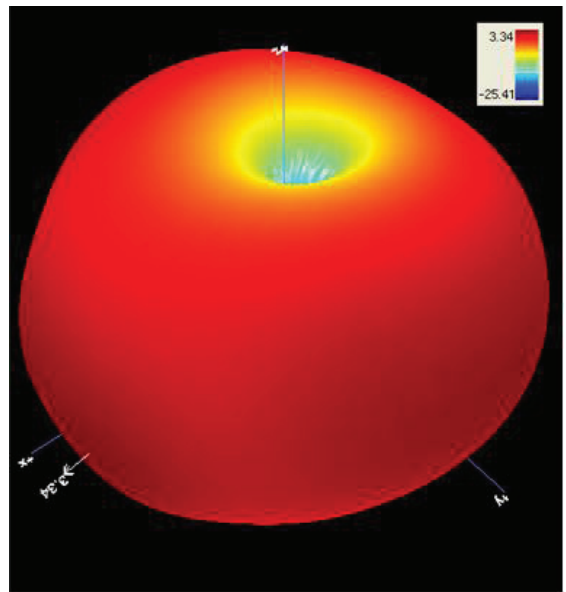


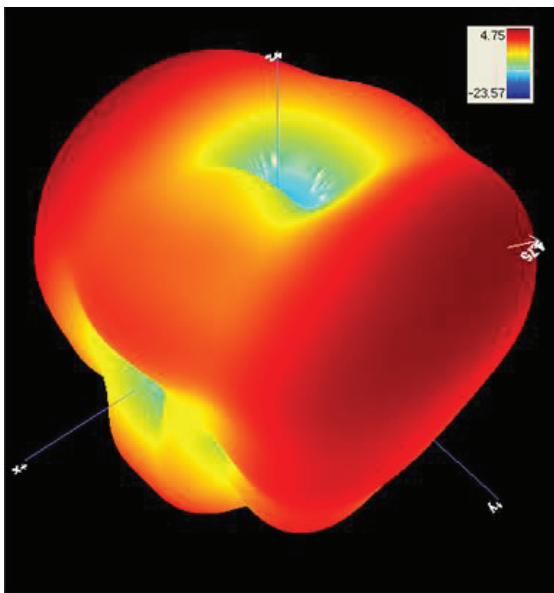
Figure 6. The simulated and measured radiation patterns at 3 GHz in the (a) xz and (b) xy planes; at 5 GHz in the (c) xz and (d) xy planes; and at 11 GHz in the (e) xz and (f) xy planes.



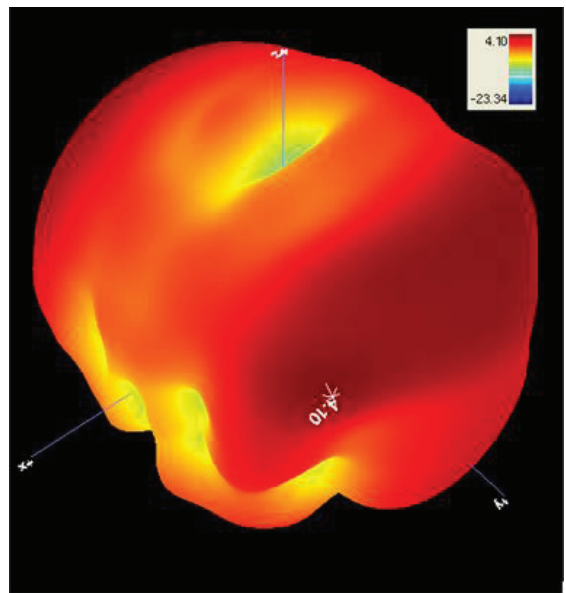
(a) 3 GHz



(b) 6 GHz



(c) 8 GHz



(d) 11 GHz

Figure 7. The measured three-dimensional radiation patterns of the UWB monopole antenna at (a) 3 GHz, (b) 6 GHz, (c) 8 GHz, and (d) 11 GHz.

3.2 Multi-Resonator

With more resonators used in the coplanar waveguide multi-resonator, more bits could be encoded into the RFID tag across the whole UWB frequency range. However, just to prove our design concept, we only used eight resonators, having resonant frequencies of 3.38 GHz, 3.64 GHz, 3.93 GHz, 4.26 GHz, 4.57 GHz, 4.86 GHz, 5.17 GHz, and 5.49 GHz, approximately evenly distributed across the frequency band from 3 GHz to 6 GHz. The results of a preliminary study on this coplanar-waveguide multi-resonator were presented in [13]. Here, the design of the multi-resonator was carried out using computer simulation, and the optimum dimensions are listed in Table 1. Figure 8 shows the prototyped coplanar waveguide multi-resonator on a Rogers substrate, RO4350B. The insertion loss (i.e., S_{21}) of the prototype was measured using a network analyzer (Agilent programmable network analyzer E5071C). Figure 9 shows the simulated and measured insertion losses. There were eight distinct resonant nulls across the UWB frequency band, which were created by the eight coplanar waveguide resonators, and could be used for encoding eight data bits for tag-identification purposes. The presence of a null could be used to represent the logic “0,” while the absence of the null could be used to represent the logic “1,” or vice versa. The spectral signature in Figure 9 could thus be used to represent a data pattern of “00000000” for a tag ID.

As mentioned before, shorting two open stubs in the coplanar waveguide resonator of Figure 2c could shift the resonance to a higher frequency. Figure 10 shows the results before and after shorting two open stubs of each of the eight coplanar waveguide resonators. It can be seen that shorting the stubs shifted bit 1 from 3.38 GHz to about 11.4 GHz, bit 2 from 3.64 GHz to 12.3 GHz, and bit 3 from 3.93 GHz to 13.4 GHz. The shifted nulls were all beyond the UWB frequency range, with much smaller insertion losses. Bits 4 to 8 were shifted to the higher frequencies beyond 14 GHz, which could not be shown in Figure 9 due to the small scale. This property could thus be used to encode different bit patterns (i.e., IDs) into the tags by shorting the stubs of different resonators. Note that in Figure 10, the resonators generated some spurious responses at frequencies about two times the corresponding resonant frequencies. However, this would not be a problem for detection because the reader, having detected a resonant frequency for a bit, could estimate the corresponding spurious response at about two times the frequency, and then easily remove (equalize) it. As a result, our design could fully use up the whole UWB frequency range.

This idea of shorting was also used in [5], where the authors used the shorting of a spiral turn of the tag’s spiral resonator shown in Figure 11 to shift the resonant frequency. The result is reproduced in Figure 12. Similar to our design, the spiral resonator had a spurious response at 4.5 GHz, slightly more than twice the resonant frequency. This design was inferior to ours in two ways, as explained in what follows. First, the insertion loss of the resonant null was only 7 dB. In contrast, for our resonators, the insertion losses of the nulls as shown in Figure 10 were larger than 19 dB, leading to better detection performance. (Note that insertion loss should always

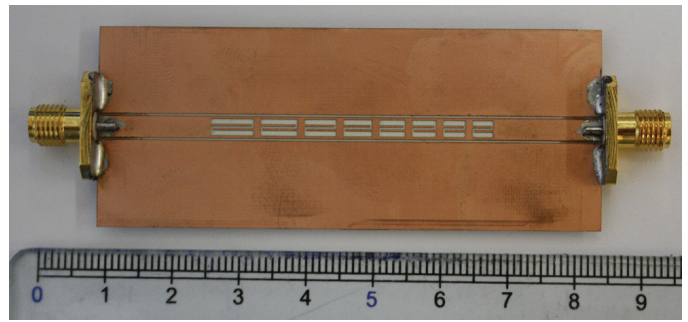


Figure 8. The prototyped eight-bit multi-resonator.

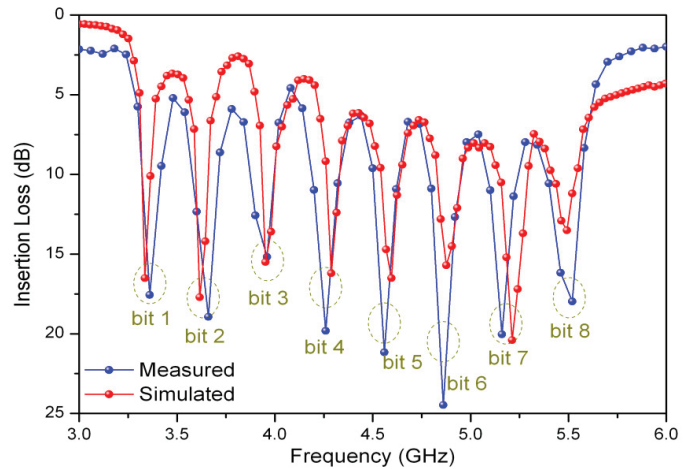


Figure 9. The measured and simulated insertion losses of the eight-bit multi-resonator.

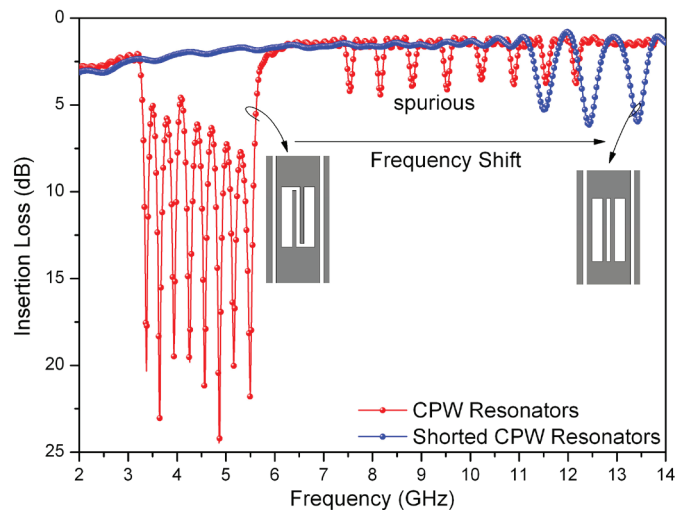


Figure 10. The simulated resonant frequencies, shifted by shorting both stubs in the coplanar waveguide resonators.

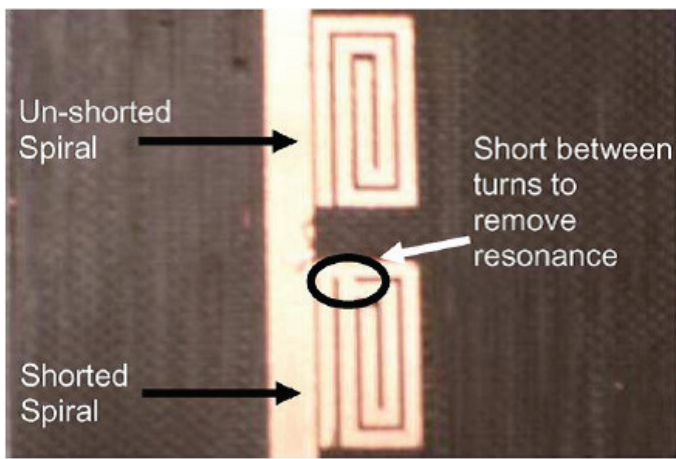


Figure 11. The tag's spiral resonator used in [5].

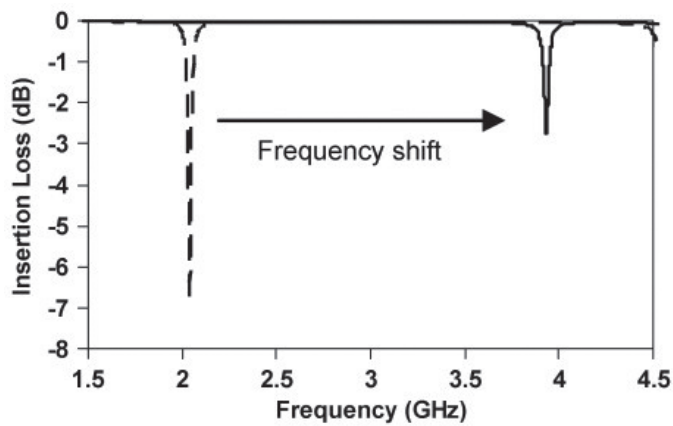


Figure 12. The frequency shift of the resonant frequency with shorting the spiral turn in [5] (the solid line is the shorted spiral; the dashed line is the non-shorted spiral).

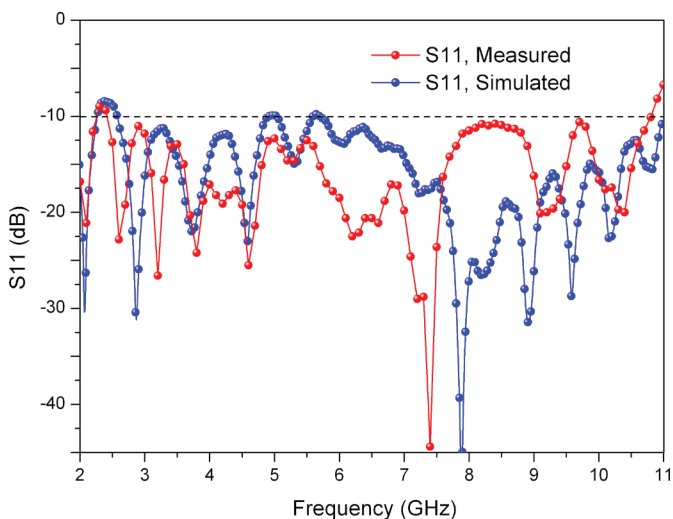


Figure 13. The measured and simulated S_{11} values of the reader's antenna.

be positive and not negative, as shown in Figure 12.) Second, Figure 11 shows that the resonant null of the spiral resonator was shifted only by a factor of about 1.85, from about 2.1 GHz to 3.9 GHz, with the insertion loss reducing to 3 dB. If the spiral resonator was designed to work, say, at 3.5 GHz in the UWB frequency range, shorting would only shift the resonance by a factor of 1.85, to about 6.5 GHz, which would still be in the UWB frequency range. Since the authors in [5] used the detection criterion of the insertion loss being larger than 1 dB, the 3 dB insertion loss of the shifted null as shown in Figure 12 could easily cause a false detection. As a result, the whole UWB frequency range could not be fully utilized, and hence a lower number of tag IDs could be accommodated.

3.3 Reader Antennas

As shown in Figures 3a and 3b, the reader antennas were fabricated using the dimensions listed in Table 2 on two Rogers substrates, each with dimensions of 180 mm \times 120 mm: see Figure 3c. The simulated and measured S_{11} values are shown in Figure 13, indicating good agreement across the UWB frequency range. The antenna had an impedance bandwidth (for $S_{11} \leq -10$ dB) from 2.25 GHz to 10.76 GHz, which not only met our RFID system-bandwidth requirement of 3 GHz to 6 GHz, but also fully satisfied the FCC UWB requirement.

The boresight gains, and one-dimensional, two-dimensional, and three-dimensional radiation patterns of the reader antenna were also studied by simulation and measurement. Figure 14a shows the simulated and measured boresight gains across the UWB frequency range. The discrepancies were mainly due to the SMA connector, which was not used in our simulation model, and the tolerances in prototype fabrication. The measured boresight gain was between 6 dBi and 10.8 dBi across the UWB frequency range. From 3 GHz to 6 GHz (which was used in the proposed RFID system), the variation was less than 2.5 dB. The measured two-dimensional radiation pattern from 2 GHz to 11 GHz in the yz plane is shown in Figure 14b, indicating more sidelobes at higher frequencies. The simulated and measured one-dimensional radiation patterns for co-polarization in the xy plane and in the xz plane at 3 GHz, 6 GHz, 8 GHz, and 11 GHz are shown in Figures 15a-15d, respectively. It can be seen that the sidelobe levels were less than -10 dB across the UWB frequency range. Figure 16 gives better views of the measured three-dimensional radiation patterns at 3 GHz, 6 GHz, 8 GHz, and 11 GHz. Although there were many sidelobes at higher frequencies, the main lobe was still quite obvious, and relatively strong.

3.4 Mutual Coupling Reduction

The effects on mutual-coupling reduction of using horizontal and vertical polarizations in the uplink and downlink, respectively, in the RFID system, and using a copper plate to separate the uplink and downlink signals, were studied by measurement. In these studies, the reader transmitting and

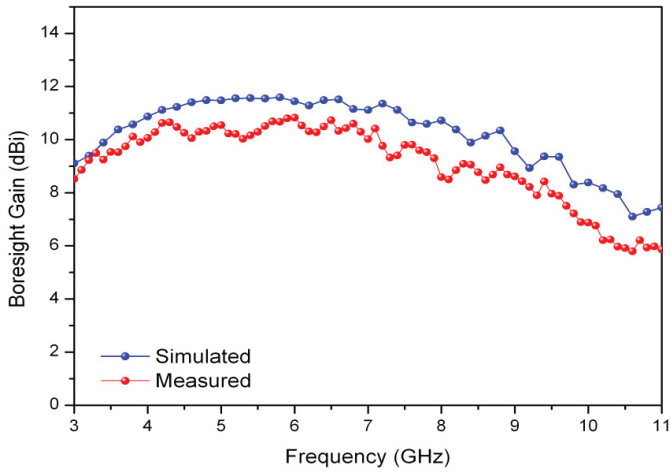


Figure 14a. The simulated and measured boresight gains of the reader's antenna.

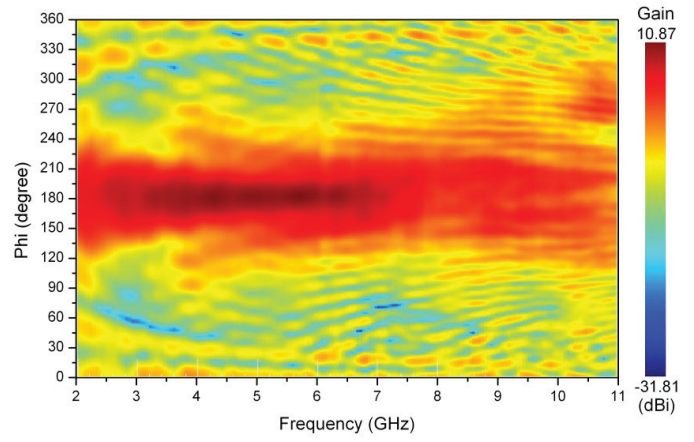


Figure 14b. The measured two-dimensional radiation pattern of the reader's antenna in the yz plane.

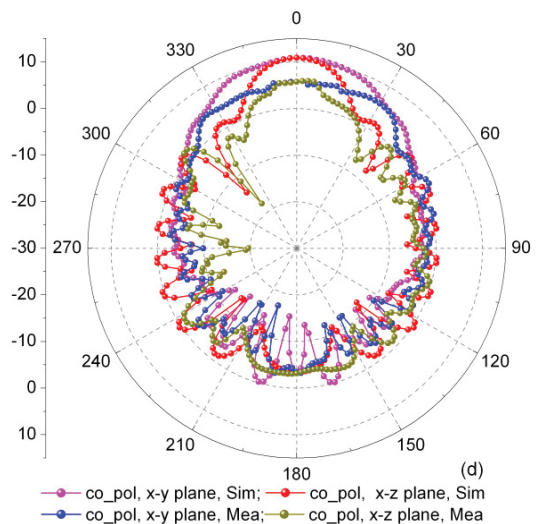
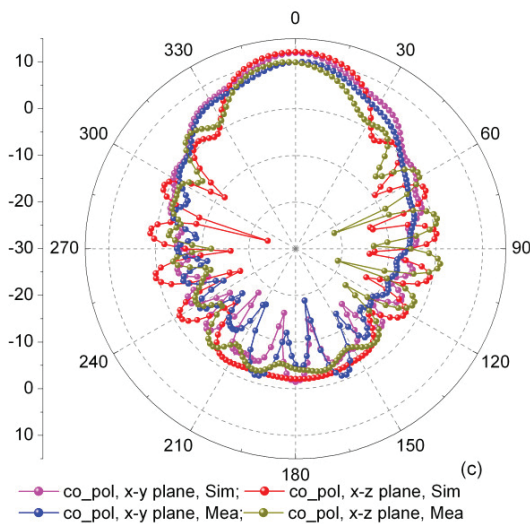
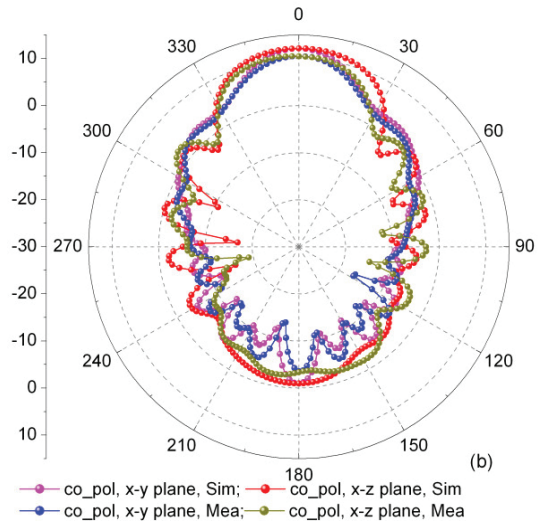
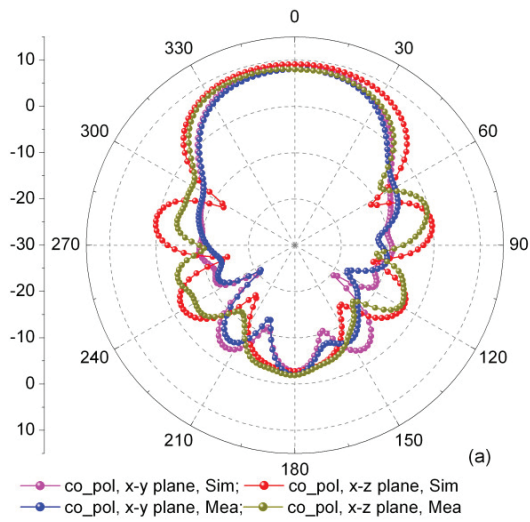
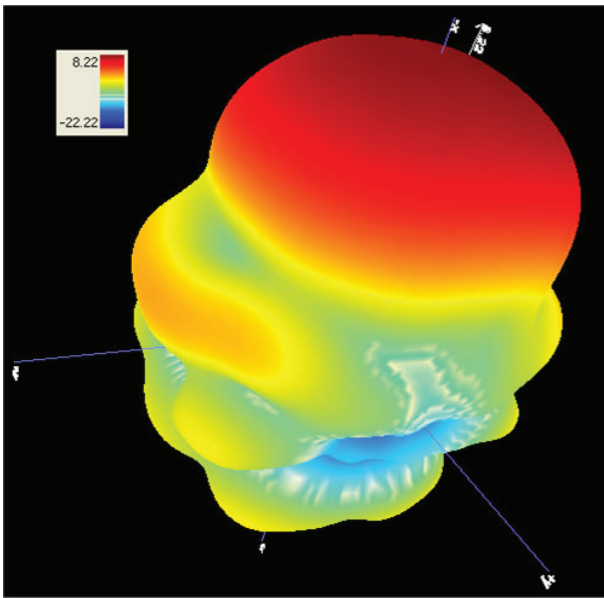
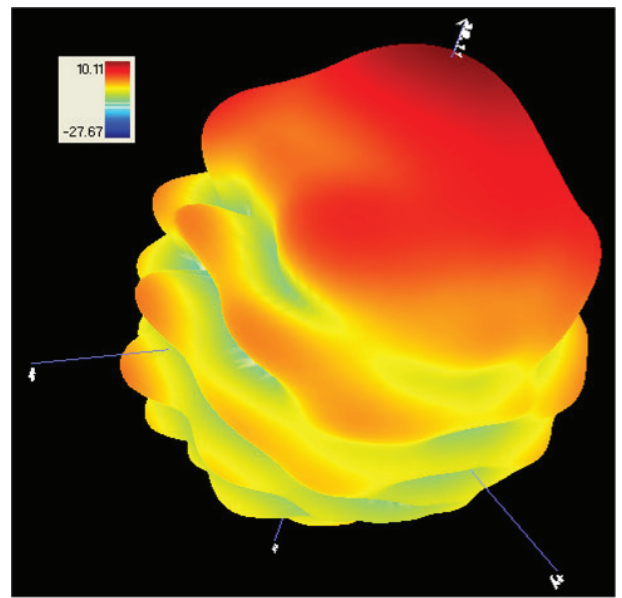


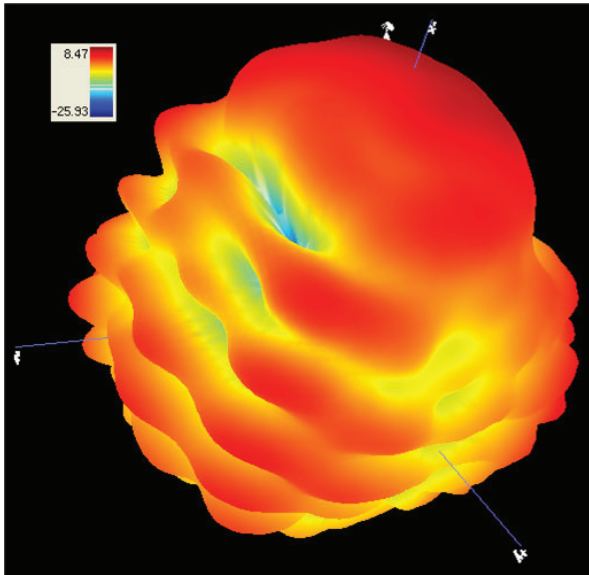
Figure 15. The measured radiation patterns of the reader's antenna in the xy plane and in the xz plane at (a) 3 GHz, (b) 6 GHz, (c) 8 GHz, and (d) 11 GHz.



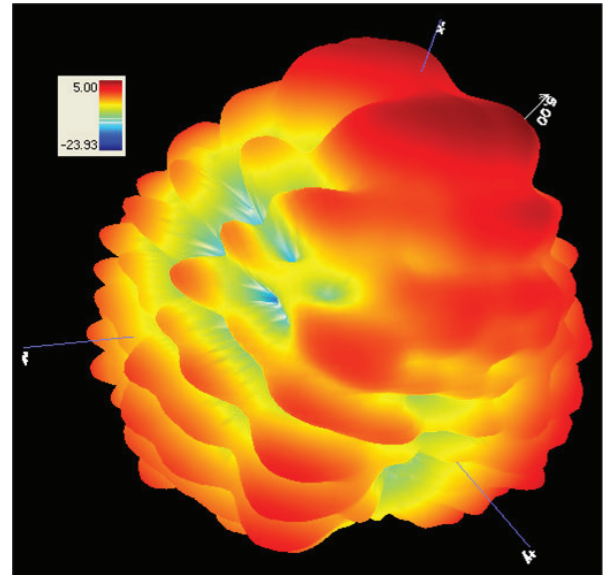
(a) 3 GHz



(b) 6 GHz



(c) 8 GHz



(d) 11 GHz

Figure 16. The measured three-dimensional radiation patterns of the reader's antenna at (a) 3 GHz, (b) 6 GHz, (c) 8 GHz, and (d) 11 GHz.

receiving antennas were placed at a distance of 12 cm apart, inside the quiet zone of the anechoic chamber. In the absence of the tag, the measured mutual coupling values (indicated by S_{21}) at the reader antenna for different arrangements are shown in Figure 17. It could be seen that when the two reader antennas were both placed in parallel and so using the same vertical polarization, the mutual coupling between them was slightly below -30 dB on average, about -20 dB at 2 GHz and -30 dB at 9 GHz. When the two reader antennas were perpendicular to each other, the mutual coupling was reduced to slightly below -40 dB across the whole frequency band. Using different polarizations in the uplink and downlink thus reduced the mutual coupling by about 10 dB more, on average. When a copper plate was used to separate the uplink and downlink signals, Figure 17 showed that the mutual coupling was further reduced by more than 10 dB, on average. Under this condition, the mutual coupling was between -50 dB to -80 dB across the frequency band tested, and about -54 dB at 3.5 GHz and -60 dB at 9 GHz. The transmitting and receiving antennas were virtually “invisible” to each other, providing a very good testing environment for our RFID system.

3.5 Measurements of the RFID System

The complete chipless tag shown in Figure 2 was fabricated on a Rogers substrate with a dimension of $L \times W = 154$ mm \times 55 mm. It was used in our RFID system of Figure 1 for measurements of S_{21} . To reduce the noise effects in the measurement environment, the RFID system was set up in the quiet zone of the anechoic chamber. Figure 18 shows a photo of the system setup, where the copper plate was removed in order to give a better view of the reader’s antennas. For measurement of S_{21} , the Agilent programmable network analyzer (E5071C), with output power set at -10 dBm, was placed outside of the chamber to reduce interference due to reflections. The reader’s antennas and the tag were mounted in fixed positions by using low-loss foam. The two reader antennas were positioned so that their boresights were pointing at the corresponding tag antennas with the same polarizations, in order to have maximum co-polarization.

The S_{21} values of the reader’s antennas, of the tag’s antennas, and of the whole RFID system varied with frequency, and these variations would affect the detection performance of the system. A reference tag without any resonator was used to eliminate these variations, and to extract the changes in S_{21} due only to the resonators (which created the spectral signature). Figure 19a shows the measured amplitudes of S_{21} for the reference tag and for two tags with IDs of 0000000 and 10101010, at a distance of 5 cm from the reader’s antennas. This distance was measured from the front edges of the Vivaldi antennas to the surfaces of the corresponding tag’s antennas. It could be seen that the S_{21} of the reference tag gradually decreased from about -30 dB at 3 GHz to about -45 dB at 6 GHz. The variation in S_{21} was due to different parts of the RFID system, and not the multi-resonator. Figure 19a shows that

for the other two tags, the S_{21} values also had a similar trend, i.e., gradually decreasing with frequency, with the eight amplitude-resonant nulls superimposed on the values. The S_{21} variation of the system made these resonant nulls less obvious than those shown in Figure 9, and this would cause difficulties in the detection of the spectral signatures. To reduce the effects of this S_{21} variation, which existed in all the tags, we subtracted the S_{21} values of the detected tags from that of the reference tag in the log scale, to obtain the amplitude difference, S_{21diff} . The results are shown in Figure 19b. It could be seen that the resonant nulls of the two tags in terms of S_{21diff} were more obvious, so the corresponding bits representing the logic “0” could be more easily detected. The S_{21diff} for the bits representing the logic “1” for the tag (ID: 10101010) were close to 0 dB, which could also be easily detected at the reader.

To study the S_{21diff} values at different distances, the tag, together with its supporting foam, was moved away from the reader’s antennas from 5 cm to 30 cm with a step size of 5 cm. This is indicated by the yellow arrows shown in Figure 18, and the moving was done without changing the orientations of either the reader’s or the tag’s antennas. The S_{21diff} of the two tags are shown in Figure 20, which indicated that as the distance increased, the S_{21diff} values became smaller. However, even at a distance of 30 cm, the spectral signature was still distinguishable. This was due to the high Q of the multi-resonator and the high isolation between the reader’s transmitting and receiving antennas. With different measured distances, the S_{21diff} values of the tag with ID: 00000000 at the null frequencies are listed in Table 3. If the maximum detectable S_{21diff} was -1 dB, as used in [5], our system had a reading range of larger than 30 cm, at least three times greater than that reported in [5].

It should be noted that although a low transmitted power of -10 dBm from the reader’s transmitting antenna was used in the measurements, the reading range could not be increased by using a higher transmitted power, for the following reason. In the presence of large interference, as in our case, the reading range was mainly determined by the signal-to-interference ratio (S/I) at the reader’s receiving antenna, and interference mainly came from the reader’s transmitting antenna.

We carried out more measurements to verify this explanation, as follows. We used a programmable network analyzer to feed a signal with a frequency spectrum from 3.995 GHz to 4.005 GHz to the reader’s transmitting antenna of the RFID system, and we used a spectrum analyzer to display the power received from the reader’s receiving antenna. (The signal with a narrow frequency spectrum from 3.995 GHz to 4.005 GHz was used in order to easily synchronize the programmable network analyzer with the spectrum analyzer for display.) The measurement was done in the absence of the RFID tag. The received powers measured by feeding transmitted powers of 10 dBm, 0 dBm, -10 dBm, and -20 dBm to the reader’s transmitting antenna are shown in Figure 21. It could be seen

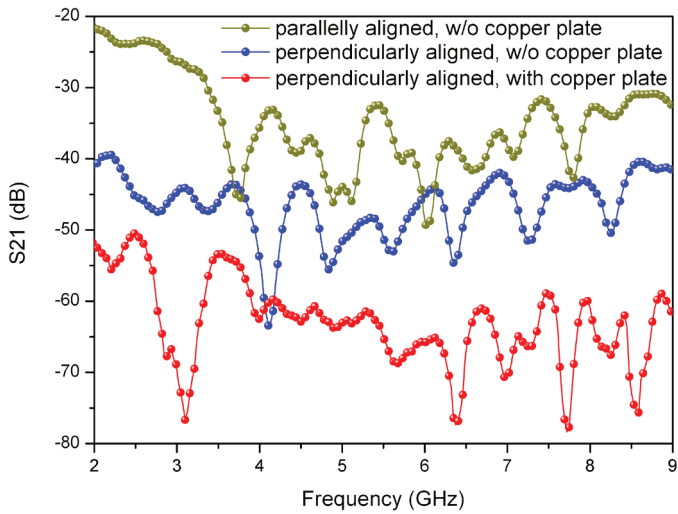


Figure 17. The measured S_{21} values (mutual coupling) of the reader's antennas in different arrangements.

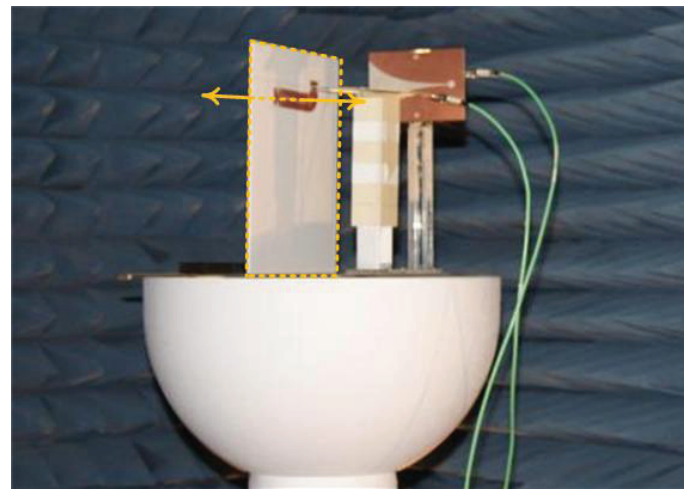


Figure 18. The UWB RFID system set up in the anechoic chamber for measurements.

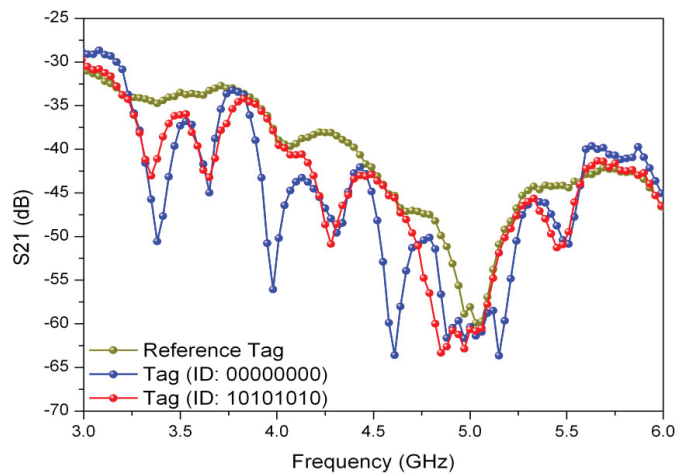


Figure 19a. The measured spectral signatures of the reference tag and of tags with IDs of 00000000 and 10101010, using amplitude difference at a distance of 5 cm.

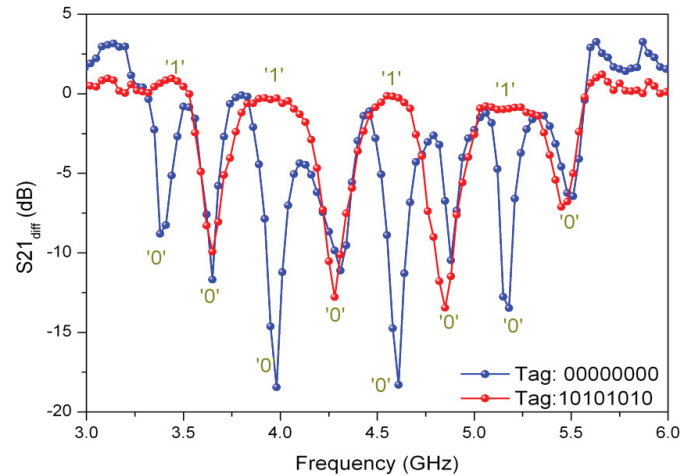


Figure 19b. The measured spectral signatures of tags with IDs of 00000000 and 10101010, using amplitude difference at a distance of 5 cm.

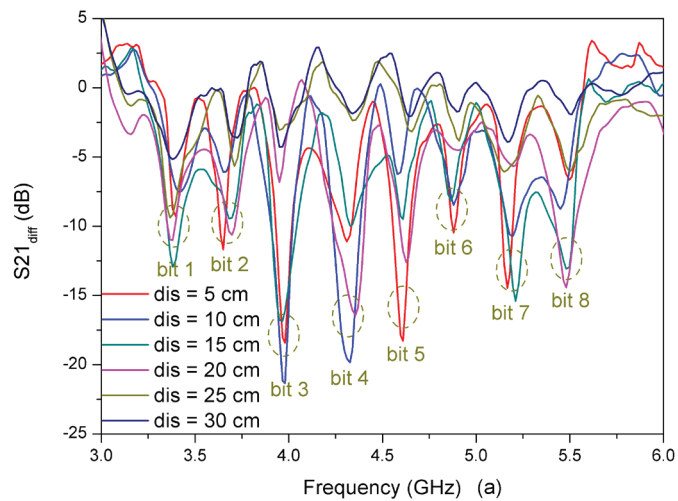


Figure 20a. The S_{21diff} values for a tag ID of 00000000 at different distances.

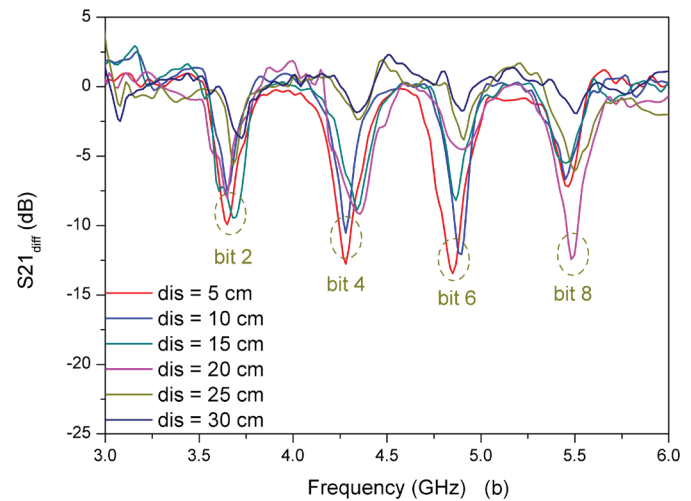


Figure 20b. The S_{21diff} values for a tag ID of 10101010 at different distances.

Table 3. The amplitude differences for the chipless tag (ID: 00000000) at different distances.

Distance	Bit 1	Bit 2	Bit 3	Bit 4	Bit 5	Bit 6	Bit 7	Bit 8
5 cm	-8.79	-11.67	-18.44	-11.11	-18.29	-10.45	-13.46	-6.43
10 cm	-7.48	-6.08	-21.33	-19.54	-6.24	-8.47	-10.61	-8.76
15 cm	-12.94	-9.44	-16.73	-9.89	-9.49	-7.69	-15.41	-13.07
20 cm	-10.99	-10.34	-3.82	-16.06	-12.22	-4.23	-4.49	-5.61
25 cm	-9.16	-5.66	-3.06	-2.35	-3.05	-3.83	-6.07	-5.92
30 cm	-5.17	-3.54	-4.27	-1.86	-2.07	-1.69	-3.87	-1.98

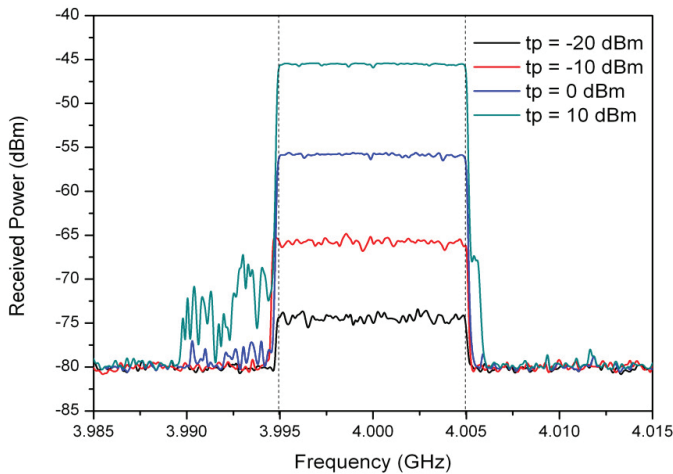


Figure 21. The powers received from the reader’s receiving antenna for different transmitted powers, t_p .

that when the transmitted power was increased by 10 dBm, the interference level at the reader’s receiving antenna was also increased by the same amount: 10 dB. As a result, the S/I remained unchanged. Note that the result for the transmitted power of -30 dBm could not be shown on the spectrum analyzer, which had the noise floor at about -80 dBm.

We also conducted the reading-range measurement when the output power from the programmable network analyzer was reduced to the minimum of -30 dBm. The results showed that the reading ranges remained the same. This was again because in the present of large interference, the reading range was determined by the S/I . At a transmitted power of -30 dBm, the interference was still quite large, and so was still the dominant factor. However, if the interference was low enough for noise to become dominant, the reading range would be determined by the signal-to-noise ratio (S/N), which was determined by the measurement environment. Under this condition, the minimum transmitted power for the RFID system would depend on the noise level of the environment, which in our case was below -100 dBm (the specification for our anechoic chamber).

If the measured distance was increased by moving the tag away from the reader, the interference would remain unchanged (for the same positions/orientations of the reader’s antennas),

but the received signal would become weaker due to the path loss, resulting in a lower S/I . The S/I was thus determined only by the measured distance, and was independent of the transmitted power.

The receiver sensitivity required to detect the resonant nulls depended on the bandwidths at the thresholds used for detection of the nulls. With a wider bandwidth, the receiver could sense the corresponding bit over a wider frequency range without making an error. However, as shown in Figure 20, different resonant nulls had different bandwidths, which also varied with the reading range and the thresholds used for detection. The receiver sensitivity thus required varied with the reading range, the threshold used for detection, and also the resonant nulls.

To study the receiver sensitivity required for each resonant null, we measured the -1.6 dB bandwidths for all the resonant nulls representing the logic “0” in Figure 20. At the shorter distances of 5 cm, 10 cm, 15 cm, and 20 cm, some resonant nulls did not have any bandwidth because the S_{21diff} values were larger than -1.6 dB. In these cases, different thresholds needed to be used. For the distances of 25 cm and 30 cm, the -1.6 dB bandwidths for different resonant nulls are shown in Table 4. It could be seen that at 30 cm, bit six had the narrowest bandwidth of only 5 MHz, and thus the receiver was required to be very accurate in frequency in order to detect the null. An offset of 2.5 MHz from the center frequency could have caused an error in detection. Bit one had the widest bandwidth of 202 MHz, and hence could have tolerated a frequency offset up to 101 MHz. At the smaller distance of 25 cm, all bits had wider bandwidths. At this distance, bit four had the narrowest bandwidth of 88 MHz, and bit one had the widest bandwidth of 284 MHz, so they could have tolerated frequency offsets of 44 MHz and 142 MHz, respectively.

Since the proposed RFID system respectively employed vertical and horizontal polarizations in the downlink and uplink to reduce interference, it was important to study the system’s tolerance to polarization mismatching between the tag’s antennas and the reader’s antennas. Studies were conducted to measure the S_{21diff} values when one of the reader’s antennas was rotated clockwise along the horizontal centerline, while keeping the tag’s orientation unchanged. At a distance of 5 cm, the measurement results for angles of rotation from 0° to 20°

Table 4. The -1.6 dB bandwidths for the chipless tag (ID: 00000000) at distances of 25 cm and 30 cm (MHz).

Distance	Bit 1	Bit 2	Bit 3	Bit 4	Bit 5	Bit 6	Bit 7	Bit 8
25 cm	284	114	126	88	93	115	291	278
30 cm	202	92	113	35	47	5	113	42

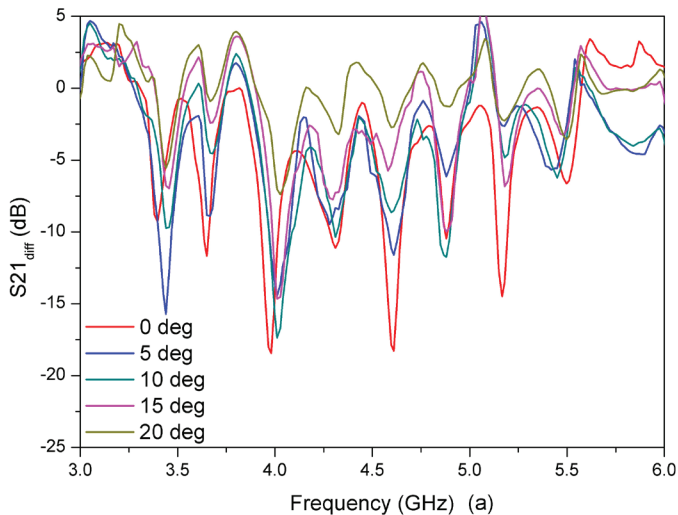


Figure 22a. The measured S_{21diff} values for a tag (ID: 00000000) with a clockwise rotation of the vertically polarized reader's antennas at a distance of 5 cm.

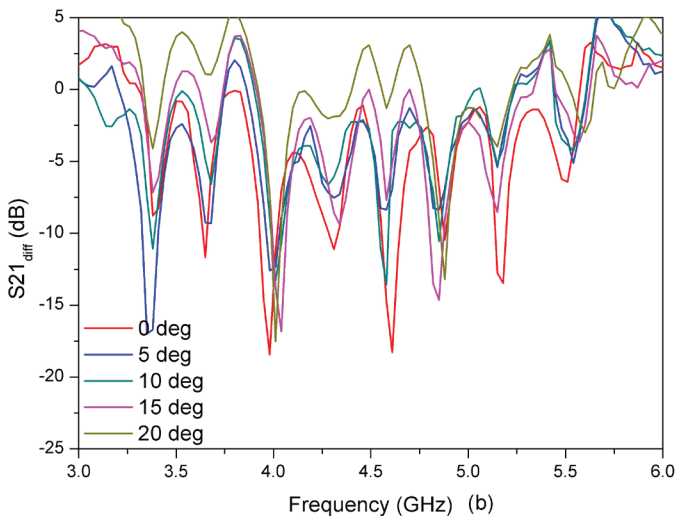


Figure 22b. The measured S_{21diff} values for a tag (ID: 00000000) with a clockwise rotation of the horizontally polarized reader's antennas at a distance of 5 cm.

with a step size of 5° for the reader's antenna are shown in Figure 22. As expected, increasing the angle of rotation decreased the S_{21diff} value. At an angle of rotation of 20° , the S_{21diff} values for some bits were above -1.6 dB. It should be noted that rotating the reader's antenna not only caused polarization mismatching between the reader's and tag's antennas, but also increased interference between the reader's antennas. If the maximum detectable S_{21diff} was -1.6 dB, the system could tolerate a rotation of about 15° for one of the reader's antennas at a reading range of 5 cm. It should be noted that at other distances, the tolerance would be less than this value.

4. Conclusions

The design of a novel chipless UWB RFID system, employing printable uniplanar chipless tags and a pair of high-gain reader antennas, has been presented. The tag ID was encoded into the spectral signature in the UWB frequency band via a coplanar waveguide multi-resonator, and could be simply programmed by shorting the open stubs of the resonators. The detection of the tag's ID was based only on the amplitude of the spectral signature, significantly simplifying the complexity of detection. Vertical and horizontal polarizations were respectively employed in the uplink and downlink signals to reduce mutual coupling. A copper plate was used at the reader to further reduce the mutual coupling. Results showed that this combination could reduce the mutual coupling by more than 20 dB. The tag's UWB antennas, the multi-resonator, and the reader's antennas were studied by computer simulation and their performance verified by measurement. Measured results of the UWB RFID system in an anechoic chamber showed that the system could achieve a reading range of at least 30 cm, much longer than the distance of 10 cm reported for a similar system. The proposed system thus has great potential for short-range item tracking at low cost.

5. References

1. K. Finkelzeller, *The RFID Handbook, Second Edition*, London, UK, John Wiley & Sons Ltd., 2003.

2. R. Want, "An Introduction to RFID Technology," *IEEE Pervasive Computing*, **5**, 1, 2006, pp. 25-33.
3. C. S. Hartmann, "A Global SAW ID Tag with Large Data Capacity," Proceedings of 2002 IEEE Ultrasonics Symposium, Munich, Germany, October 2002, pp. 65-69.
4. V. Plessky and L. Reindl, "Review on SAW RFID Tags," *IEEE Transactions on Ultrasonics, Ferroelectric and Frequency Control*, **57**, 2010, pp. 654-668.
5. S. Preradovic, and N. C. Karmakar, "Multiresonator-Based Chipless RFID System for Low-Cost Item Tracking," *IEEE Transactions on Microwave Theory and Techniques*, **57**, 5, May 2009, pp. 1411-1419.
6. S. Preradovic, and N. C. Karmakar, "Design of Chipless RFID Tag for Operation on Flexible Laminates," *IEEE Antennas and Wireless Propagation Letters*, **9**, 2010, pp. 207-210.
7. S. Preradovic, and N. C. Karmakar, "Multiresonator Based Chipless RFID Tag and Dedicated RFID Reader," 2010 IEEE International Microwave Symposium Digest, Anaheim, CA, May 2010, pp. 1520-1523.
8. S. Hu, Y. Zhou, C. L. Law, and W. Dou, "Study of a Uniplanar Monopole Antenna for Passive Chipless UWB-RFID Localization System," *IEEE Transactions on Antennas and Propagation*, **AP-58**, 2, February 2010, pp. 271-278.
9. A. Lazaro, A. Ramos, D. Girbau, and R. Villarino, "Chipless UWB RFID Tag Detection Using Continuous Wavelet Transform," *IEEE Antennas and Wireless Propagation Letters*, **10**, 2011, pp. 520-523.
10. "Federal Communications Commission Revision of Part 15 of the Commission's Rules Regarding Ultra-Wideband Transmission Systems," FCC, 2002, First Report and Order FCC, 02.V48.
11. D. Dardari, R. D'Errico, C. Roblin, A. Sibille, and M. Z. Win, "Ultrawide Bandwidth RFID: The Next Generation?," *Proceedings of the IEEE*, **98**, 9, September 2010, pp. 1570-1582.
12. Y. F. Weng, S. W. Cheung, and T. I. Yuk, "Ultra-Wideband Antenna Using CPW Resonators for Dual-Band Notched Characteristic," 2009 International Conference on Wireless Communications and Signal Processing, Nanjing, China, November 2009.
13. Y. F. Weng, S. W. Cheung, and T. I. Yuk, "A Printable Uniplanar Chipless UWB-RFID Tag Using Multiple Resonators," The 3rd International EURASIP Workshop on RFID Technology, Cartagena, Spain, September 2010.
14. P. J. Gibson, "The Vivaldi Aerial," 9th European Microwave Conference, Surrey, England, September 1979, pp. 101-105.
15. Y. Huang and K. Boyle, *Antennas from Theory to Practice*, New York, John Wiley & Sons, 2008.
16. S. W. Qu, J. Li, and Q. Xue, "A Band-Notched Ultrawideband Printed Monopole Antenna," *IEEE Antennas and Wireless Propagation Letters*, **5**, 1, 2006, pp. 495-498.
17. M. Houdart, "Coplanar Lines: Application to Broadband Microwave Integrated Circuits," Proceedings of 6th European Microwave Conference, Rome, Italy, September 1976, pp. 49-53.
18. X. Y. Wu, I. Awai, Z. Yan, K. Wada, and T. Moriyoshi, "Quality Factors of Coplanar Waveguide Resonators," 1999 Asia Pacific Microwave Conference, **3**, November 1999, pp. 670-673.
19. E. Thiele and A. Taflove, "FD-TD Analysis of Vivaldi Flared Horn Antennas and Arrays," *IEEE Transactions on Antennas and Propagation*, **AP-42**, 5, May 1994, pp. 633-641.
20. J. Shin and D. H. Schaubert, "A Parameter Study of Strip-line-Fed Vivaldi Notch-Antenna Arrays," *IEEE Transactions on Antennas and Propagation*, **AP-47**, 5, May 1999, pp. 879-886.
21. Z. N. Chen, M. J. Ammann, X. Qing, X. H. Wu, T. S. P. See, and A. Cai, "Planar Antennas," *IEEE Microwave Magazine*, **7**, 6, December 2006, pp. 63-73.

Introducing the Feature Article Authors

Y. F. Weng received the BSc from Zhejiang University, China, in 2006, and the PhD from the University of Hong Kong. From 2005-2007, he worked as a Hardware Engineer in Shanghai Xinao Communication Technology Ltd. His research interests include UWB antennas and RFID systems.




S. W. Cheung received the BSc with First Class Honours in Electrical and Electronic Engineering from Middlesex University, UK, in 1982, and the PhD from Loughborough University of Technology, UK, in 1986. From 1982 to 1986, he was a research assistant in the Department of Electronic and Electrical Engineering at Loughborough University of Technology, where he collaborated with Rutherford Appleton Laboratory and many UK universities to work a project for new generations of satellite systems.

Dr. Cheung is an Associate Professor at the University of Hong Kong and in charge of the Microwave, RF Frequency, and Telecom Laboratories. His current research interests include antenna designs; 2G, 3G, and 4G mobile communications systems; MIMO systems; and satellite communications systems. He is a Senior Member of the IEEE, and has been serving the IEEE in Hong Kong for the past twenty years. In 2009 and 2010, he was the Chair of the IEEE Hong Kong Joint Chapter on Circuits and Systems and Communications. Since 2011, he has been the Treasurer of the IEEE Hong Kong Section and has helped in organizing different international conferences.



T. I. Yuk received his BS from Iowa State University in 1978, and his MS and PhD from Arizona State University in 1980 and 1986, respectively. Since 1986, he has been teaching at the University of Hong Kong. His current research interests include wireless communications and antenna designs.



Liu Li received the BSc from the University of Electronic Science and Technology of China in 2009. She is currently working towards her PhD at the University of Hong Kong. Her research interests include RF and microwave circuits, antenna designs, and MIMO systems. 

AP-S Election Results

The following are the results of the elections for the IEEE Antennas and Propagation Society for positions beginning in 2013:

2013 President Elect

Tapan K. Sarkar

Members of the AdCom (2013-2015)

Ahmed A. Kishk

Dirk Manteuffel

Levent Sevgi

Leena Ukkonen

Changes of Address or Delivery Problems

Information regarding subscriptions and addresses is managed by IEEE headquarters. It is *not* maintained, nor can it be changed, by any member of the *Magazine* staff. If you are a member of the IEEE, your subscription is sent to the address in your IEEE member record. Your address can be confirmed or updated by visiting the Web page dealing with delivery of IEEE publications:

<http://www.ieee.org/about/help/subscriptions.html>

This page also has information about publication delivery, and a link to an online form that can be used to inquire about missing or delayed publications:

http://www.ieee.org/about/help/publication_inquiry.html

You can also update your address information by contacting IEEE headquarters: Member Address Records, IEEE Headquarters, 445 Hoes Lane, Piscataway NJ 08855-1331 USA; Tel: +1 (908) 981-0060 or +1 (800) 678-4333; Fax: +1 (908) 981-9667; E-mail: address.change@ieee.org. If you are an institutional or other non-member subscriber, contact IEEE Customer Service at the above address, telephone, and fax numbers; E-mail: customer.service@ieee.org.

Please do *not* send requests related to the above items to any member of the *Magazine* Staff.